Continuous Flow Acoustofluidics in Wall-less Capillary Bridge Channels

Sadaf Maramizonouz[1,2], Jeremy J. Hawkes[3,2], Mohammad Rahmati[2,*], Yong-Qing Fu[2,*]

[1] School of Engineering, Newcastle University, Newcastle upon Tyne, NE1 7RU, UK.

[2] Faculty of Engineering & Environment, Northumbria University, Newcastle upon Tyne, NE1 8ST, UK.

[3] Acoustic Machines, Liverpool, L25 4TQ, UK.

[*]Corresponding Authors:

Dr. Mohammad Rahmati, E-mail: mohammad.rahmati@northumbria.ac.uk

Prof. Richard Yongqing Fu, E-mail: richard.fu@northumbria.ac.uk

Abstract

In this study, the manipulation, patterning, and alignment of yeast particles were successfully demonstrated inside a continuous flow capillary bridge channel. A numerical model is presented to explore various frequencies and channel configurations, and the numerical results are compared to the experimental findings. The numerical model produced results in excellent agreement with the experimental data. Yeast particles were aligned in linear patterns while continuously flowing parallel to the air-water interfaces of the capillary bridge channel. The width of the fluid-guide significantly affected the acoustic pressure fields and thus the quality of particle patterning. Most frequencies can achieve particle alignment inside the capillary bridge channel, while the liquid flow straightens the particle line. Studies of ultrasound transfer from a solid wave-guide into the liquid in a capillary bridge channel have previously shown that some nodes which formed in the waveguide will cross the solid-fluid interface into the water of the capillary bridge. The nodes formed by this extension mechanism are not easily distinguishable from nodes formed by a resonance in the liquid since particles are attracted to them in the same way and the node-to-node separation is often similar. This paper provides further foundation for the new node extension concept and identifies some of its unique features

1 Introduction

Continuous flow acoustofluidics synergizes acoustics and microfluidics to manipulate particles and biological cells within microchannels. It has previously been successfully utilised for aligning [1], focusing [2], sorting and capturing of biological cells or bacteria [3, 4] and separating platelets [5], blood cells [6], cancer cells [2], and other types of biological organisms [7, 8]. These continuous flow acoustofluidic systems offer various advantages including small and compact sizes, precise control over the particles' movement and position, and label-free and contact-free manipulation, conserving the viability, proliferation, and function of biological organisms [2, 6]. Recent advances in the field of continuous flow

acoustofluidics presents efficient automated separation of platelet-reduced plasma from whole blood without the need for external labelling [9], as well as sorting of cells based on their sizes and mechanical properties, achieving high efficiency, purity, and viability in the separated populations [10].

However, most of these devices require large power supplies, complex designs, and clean room manufacturing facilities, all of which are complicated and expensive [11, 12]. Developing, designing, and implementing alternatives to traditional microchannels that can streamline the fabrication process, lower production costs, and shorten manufacturing time, which currently presents a great potential and to entice new researchers to modify and enhance the current technology for commercial purposes outside laboratory settings [12].

One novel approach to simplify the fabrication process and understand acoustofluidic mechanisms is based on the utilisation of wall-less microfluidic devices by employing capillary bridge channels [13]. Capillary bridges can easily be formed by any liquid between two solid walls, in our system these are the top and bottom walls of the channel. Fluid is held either stationary or flowing in the gap between the walls. Such channels can be formed between a large surface separated by up to 2 mm from a narrow wall so that the narrow wall acts as a fluid-guide. When used in microfluidic systems the narrow wall is often called a fluid-guide and can take many forms for example a flat surface [13, 14], and an array of apertures such as micro-rings [15] or electrodes [16]. In acoustofluidics, the advantage of the capillary bridge [13] is the absence of walls on either side of the channel which avoids the possibility of sound transmission through the side wall to the fluid-guide. This produces less acoustically complex system than systems with enclosed channels.

This paper demonstrates a continuous flow acoustofluidic capillary bridge. It builds on the previous work which showed that the nodes in the liquid capillary bridges are often extensions of nodes formed in the solid wave-guide [13]. The continuous flow acoustofluidic capillary bridge system is then utilised for acoustic manipulation, patterning, and alignment of continuously flowing yeast particles.

2 Experimental Investigation

The continuous flow capillary bridge acoustofluidic system comprises of the following components:

- A polystyrene strip at the bottom as the fluid-guide; Five fluid-guides with a length of 40 mm and widths of 0.5 mm, 1 mm, 2.5 mm, 3 mm, and 18 mm, with one hole at each end of the strip acting as inlet and outlet, were cut from a 0.05 mm polystyrene film (additive free biaxially orientated ST31-FM-000150, Goodfellow, UK) using a plotter cutter (Brother ScanNCut CM900);
- A glass microscope slide at the top as the wave-guide;
- A 3D-printed holder to hold the fluid-guide under tension from both ends along its length using fasteners screwed in place in order to create a flat surface for the fluid to flow along

the capillary bridge. The holder was also used to fix the position of the wave-guide above the fluid-guide setting the height of the channel as 0.75 mm or 1 mm using pins with each corresponding height and to facilitate the connection of the wave-guide to the acoustic wave source;

- A side mounted piezoelectric transducer disk made from lead zirconate titanate (a.k.a. lead zirconium titanate) commonly called PZT (CAS number 12626-81-2), used as an acoustic wave source. It had an electrode with a 25 mm diameter on the front face and another electrode with a 12.5 mm diameter on the back face, a thickness of 2 mm, and a nominal operating frequency of 1.035 MHz (with the higher harmonic frequency values of 3.34 MHz, 5.57 MHz, and 7.58 MHz, etc.);
- A radio frequency (RF) function generator (Agilent 33220A) connected to a power amplifier (ENI 240L) to generate the amplified RF signals with the appropriate frequencies and supply he signals to the PZT disk;
- A syringe pump (ExiGo pump) to introduce the fluid-particle suspension into the capillary bridge system;
- Samples of yeast particle (*S. Cerevisiae*, Allinson, UK) with a radius of ~2.5 μm [17] suspended in deionised (DI) water diluted to reach a cell concentration of ~10^7 ml^{-1} to visualise the particle patterning and alignment. The properties of yeast particles and DI water are presented in **Table 1**.

Table 1 *The properties of yeast particles [17] and DI water to 21° room temperature.*

Material	**Density (**kg/m^3**)**	**Compressibility (**Pa^{-1}**)**	**Viscosity (**Pa.s**)**
DI water	998	5×10^{-10}	1×10^{-3}
Yeast Particles	1100	3.3×10^{-10}	-

Each experiment is started by introducing the fluid-particle suspension into the wall-less channel by pumping it through the inlet hole located on the fluid-guide using the syringe pump. The suspension then flows on the surface of the fluid-guide along its path, forming a capillary bridge channel between the fluid-guide and the wave-guide located at the top. Two free surfaces of the fluid in contact with the surrounding air at both sides (i.e., air-water interfaces) comprise the channel side walls. During the continuous flow experiments, a fluid flow rate of 2.5 μl/s was sustained, enforce by the syringe pump. The liquid exited the capillary bridge channel through the outlet hole located on the fluid-guide and was collected in a vial.

After establishing a steady and stable flow, the wave-guide was driven using the acoustic wave source (the PZT disk) by applying the amplified RF signals with the appropriate frequencies using the RF function generator and amplifier. The acoustic waves were generated by the PZT disk and propagated into the wave-guide, then leaked into the liquid. The acoustic force then acted on the yeast particles and pushed them towards the pressure nodes of the acoustic field to form continuously flowing linear patterns inside the wall-less channel.

The air-water walls (the interfaces between the liquid inside the capillary bridge channel and the air) were maintained with negligible deformation at the flow rate and the acoustic power

used. All the experiments were conducted at room temperature (~21°).

Figure 1(a) illustrates a three-dimensional (3D) schematic of the designed continuous flow capillary bridge channel integrated with a side-mounted PZT disk to form an acoustofluidic device. **Figures 1(b-1)** and **(b-2)** schematically show the capillary bridge setup and the particle/cell patterns formed inside the channel from the cross-sectional and top views, respectively. At the interface of the wave-guide and the liquid (the green circles in **Figure 1(b-1)**), the contact line of the capillary bridge is pinned because of contact angle hysteresis since the acoustic force is not sufficient to overcome the contact line pinning. For the fluid-guide, the liquid contact line (the blue circles in **Figure 1(b-1)**) is pinned by the edge of the fluid-guide. Complete details on the construction of the experimental set-up can be found in [13, 18].

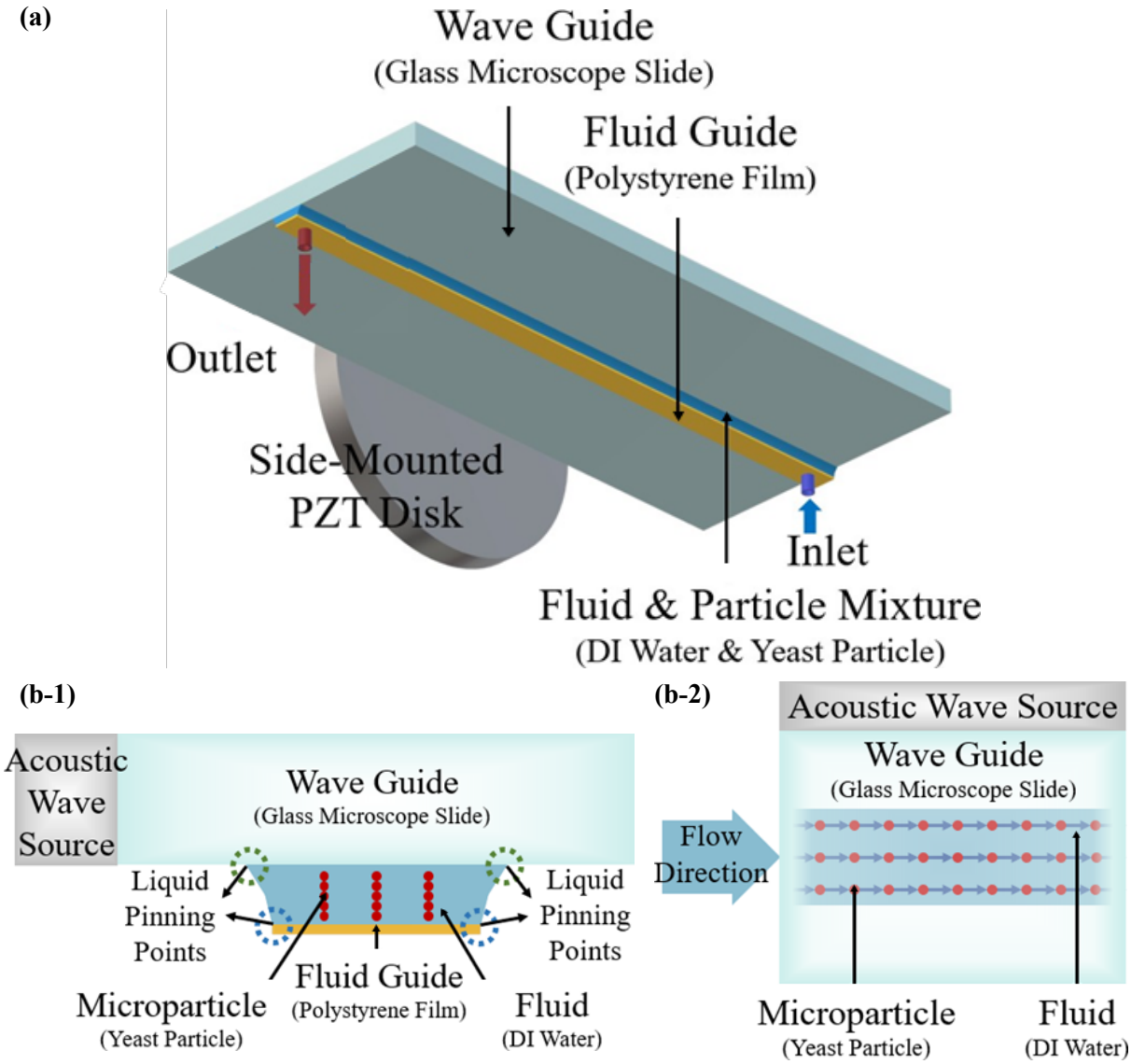

Figure 1 (a) *Schematic illustrations of the continuous flow capillary bridge acoustofluidic system showing three-dimensional views of the components for a side mounted PZT setup,* ***(b-1)*** *cross-sectional view, and* ***(b-2)*** *top view of particle patterning,*

3 Numerical Modelling

An acoustofluidic set-up is a multi-physics system consisting of the acoustic fields, the fluid flow, the solid mechanics, the piezoelectric effects, and the particle dynamics. Acoustic wave propagation in liquids induces oscillatory pressure and velocity fields that influence the liquid's field variables. While the liquid's compressibility is often negligible in hydrodynamics due to low fluid velocities, it drives acoustic wave propagation because of the stark differences in length and time scales between the phenomena. Acoustic waves operate on scales of ~10^{-9} m and ~10^{-8} s, whereas the liquid operates on ~10^{-3} m and ~1 s. Despite their small magnitude, these acoustic fluctuations in pressure and velocity are critical in acoustofluidics. Direct Numerical Simulation (DNS) is, in theory, the most accurate approach for modelling acoustofluidic systems, solving the compressible Navier-Stokes equations to fully capture the multi-physics interactions across diverse scales. However, DNS is computationally expensive, requiring extremely fine grids to resolve small-scale interactions which is often impractical. To address this, perturbation methods offer an efficient and practical alternative, reducing computational demands while maintaining accuracy. These methods treat the acoustic field's oscillatory effects as small-scale perturbations superimposed on the fluid's unperturbed state. The resulting field variables are represented as a combination of zeroth-order (unperturbed) and first-order (perturbed) approximations [19, 20].

To understand the details of the current acoustofluidic set-up and the behaviour of the particles under acoustic agitations, the theory and governing equations for the continuous-flow capillary bridge system were described.

3.1 The Theoretical Analysis

The acoustic field generated inside the capillary bridge system was modelled using the Helmholtz equation [21]:

$$\boldsymbol{\nabla}^2 P(\boldsymbol{r}) + \frac{\omega^2}{{c_f}^2} P(\boldsymbol{r}) = 0 \qquad (1)$$

where $P(\boldsymbol{r})$ is the wave pressure field as a function of position vector $\boldsymbol{r}$, ω is the wave angular frequency, and $c_f = \sqrt{\left(\frac{\partial P}{\partial \rho}\right)_s}$ is the wave speed in the fluid. The boundary conditions on the walls of the acoustic were defined as impedance boundary condition $Z_{wall} = \rho_{wall} c_{wall}$, where Z_{wall} is the wall's impedance, ρ_{wall} is the wall density, and c_{wall} is the wave's propagation velocity in the wall [21]. The impedance boundary condition is usually used to model how the acoustic waves are interacted with the interfaces between different media by incorporating the effects of material properties and boundary behaviours [21].

The fluid flow was considered steady in time, laminar, incompressible, and viscous and Navier-Stokes equations were used to model the fluid flow [21, 22]:

$$\boldsymbol{\nabla}.\boldsymbol{U}_f = 0 \qquad (2)$$

$$\rho_f \left((\boldsymbol{U}_f . \boldsymbol{\nabla}) \boldsymbol{U}_f \right) = -\boldsymbol{\nabla} P + \mu_f \boldsymbol{\nabla}^2 \boldsymbol{U}_f \quad (3)$$

where $\boldsymbol{U}_f$ is the fluid velocity vector, ρ_f is the fluid density, P is the fluid pressure and μ_f is the fluid viscosity. The boundary conditions of the fluid domain included the inlet and outlet boundary conditions defined as fixed volume flow rate and fixed pressure, respectively. At the interface of water with the wave-guide and the fluid-guide, a no-slip boundary condition ($\boldsymbol{U}_{fluid} = \boldsymbol{U}_{wall}$) was defined [22]. The boundary condition for modelling the air-water interfaces depends on whether the air-water interface is free or rigidified. For the free interfaces, the boundary conditions include shear stress continuity across the interface. Whereas for the rigidified interfaces, the boundary conditions are no-slip. A rigidified interface can occur when dust, microparticles, or surfactants are adsorbed at an air-water interface which was observed to happen during the experiments. Here, we assume that the air-water interfaces are rigidified, and no-slip boundary conditions can be used to model the fluid flow. This means that the drag for fluid flow through the capillary bridge channel can be modelled as if the walls were solid.

All the solid parts (including the fluid-guide and the wave-guide) were modelled using the Hooke's Law as the governing equation [21]:

$$\boldsymbol{\sigma} = E \boldsymbol{\varepsilon} \quad (4)$$

$$\boldsymbol{\varepsilon} = \frac{1}{2} [\boldsymbol{\nabla} \boldsymbol{U}_s + (\boldsymbol{\nabla} \boldsymbol{U}_s)^T] \quad (5)$$

$$\boldsymbol{\nabla} . \boldsymbol{\sigma} + \boldsymbol{F}_s = 0 \quad (6)$$

where $\boldsymbol{\sigma}$ is the stress tensor of the solid part, E is the Young's modulus of the solid part, $\boldsymbol{\varepsilon}$ is the strain tensor of the solid part, $\boldsymbol{U}_s$ is the displacement vector of the solid part, and $\boldsymbol{F}_s$ is the pressure effect on the solid part which is caused by wave propagation in the fluid per unit volume of the solid [19]. It is worth mentioning that **Equation (5)** is an approximation of the full formula, simplified for the ease of calculation.

The piezoelectric effects were modelled using the Maxwell's equations given below [23]:

$$\boldsymbol{\varepsilon} = \boldsymbol{s}\boldsymbol{\sigma} + \boldsymbol{d}\boldsymbol{E} \quad (7)$$

$$\boldsymbol{D} = \boldsymbol{d}\boldsymbol{\sigma} + \boldsymbol{p}\boldsymbol{E} \quad (8)$$

$$\boldsymbol{E} = -\boldsymbol{\nabla} \mathbf{V} \quad (9)$$

$$\boldsymbol{\nabla} . \boldsymbol{D} = q \quad (10)$$

where $\boldsymbol{s}$ is the fourth order tensor of mechanical compliance, $\boldsymbol{d}$ is the third order tensor of piezoelectric charge constant, $\boldsymbol{E}$ is the electric field, $\boldsymbol{D}$ is the first order tensor of electric displacement, $\boldsymbol{p}$ is the second order tensor of permittivity, $\boldsymbol{\nabla}$ is the electric potential and q is the electric charge concentration [23].

The governing equations of particle's dynamics utilizing the Euler-Lagrange approach can be written as follows for a single particle [24]

$$\frac{\partial \boldsymbol{X}_p}{\partial t} = \boldsymbol{U}_p \quad (11)$$

$$\frac{\partial \rho_p \boldsymbol{U}_p}{\partial t} = \boldsymbol{W} + \boldsymbol{D} + \boldsymbol{F}_{AR} \quad (12)$$

where $\boldsymbol{X}_p$ is the particle's position vector, $\boldsymbol{U}_p$ is the particle velocity vector, $\boldsymbol{W} = (\rho_p - \rho_f)\boldsymbol{g}$ is the gravity and buoyancy force, $\boldsymbol{g}$ is the gravitational acceleration, $\boldsymbol{D}$ is the drag force acting on the particle (refer to **Equation (13)**), and $\boldsymbol{F}_{AR}$ is the acoustic force acting on the particle (refer to **Equation (14)**).

The drag force that the particles experienced when moving through the fluid depends on the properties of the fluid, the properties of the particles, and the velocity of the particle relative to the flow and for spherical particles is given by the Stokes' drag law [24]:

$$\boldsymbol{D} = \rho_p \frac{\boldsymbol{U}_f - \boldsymbol{U}_p}{\tau_p} \quad (13)$$

Where ρ_p is the particle density, $\tau_p = \rho_p d^2/18\mu_f$ is the particle characteristic time which is the time the particle takes to respond to a velocity change, and d is the particle's diameter [24].

The acoustic force applied to a particle in an acoustic field can be calculated using the following equations [25-28]:

$$F_{AR} = (\frac{\pi {P_{ac}}^2 \forall_p \beta_f}{2\lambda}) \emptyset_s(\rho) \sin(2k\tilde{d}) \quad (14)$$

$$\emptyset_s(\rho) = \frac{5\rho_p - 2\rho_f}{2\rho_p + \rho_f} \quad (15)$$

where P_{ac} is the acoustic pressure amplitude, $\forall_p$ is the particle volume, β_f is the fluid compressibility, λ is the wavelength, k is the wave number, and $\tilde{d}$ is the particle's distance from the nearest pressure node (or anti-node) along the wave propagation direction. The acoustic force directs the particles towards either the pressure node (the minimum pressure amplitude) or the pressure antinode (the maximum pressure amplitude), depending on the physical and mechanical properties of fluid and particle. $\emptyset_s$ is called the acoustic contrast factor and its sign defines whether each particle moves towards the pressure node ($\emptyset_s$>0) or the pressure antinode ($\emptyset_s$<0) under the effect of acoustic force [25-28]. The yeast particles used in this study were driven to the pressure nodes.

To predict the behaviour of the whole 3D system, accurately modeling the interactions at fluid-solid interfaces is crucial, where the vibration of the solid surface affects the fluid and the acoustic pressure field inside the fluid causes a pressure effect on the solid surface. In our designed acoustofluidic system, the ultrasound caused vibration of the glass plate, which in turn caused the propagation of sound waves into the fluid. In this case a "two-way coupling" between the fluid channel and the solid walls was used to simulate the system which included the structural acceleration as experienced by the fluid and the fluid load on the solid walls [25-28].

3.2 The Numerical Model

The geometry was defined as a three-dimensional set-up of the acoustofluidic device including

the PZT disk, the wave-guide, the fluid-guide, and the fluid inside the channel. The shape of the air-water interfaces can be considered either vertical or a meniscus. Both geometries were used to model the air-water walls and comparison of the results showed that there were no apparent differences in how the air-water walls were modelled. For the results presented in this research, the air-water walls were modelled as a meniscus with contact angles of 0° and 90° for the fluid-guide and the wave-guide, respectively. The computational domain was discretised using ~550,000 hexahedron (for the fluid-guide, the wave-guide, and the liquid) and tetrahedron (for the PZT disk) elements. The modelled geometry and mesh are shown in **Figure 2(a)**.

Mesh dependency analysis was performed to show that the computational grid is fine enough so that it does not influence the acoustic pressure field while maintaining a reasonable computational time. Results of mesh dependency analysis is presented in **Figure 2(b)**.

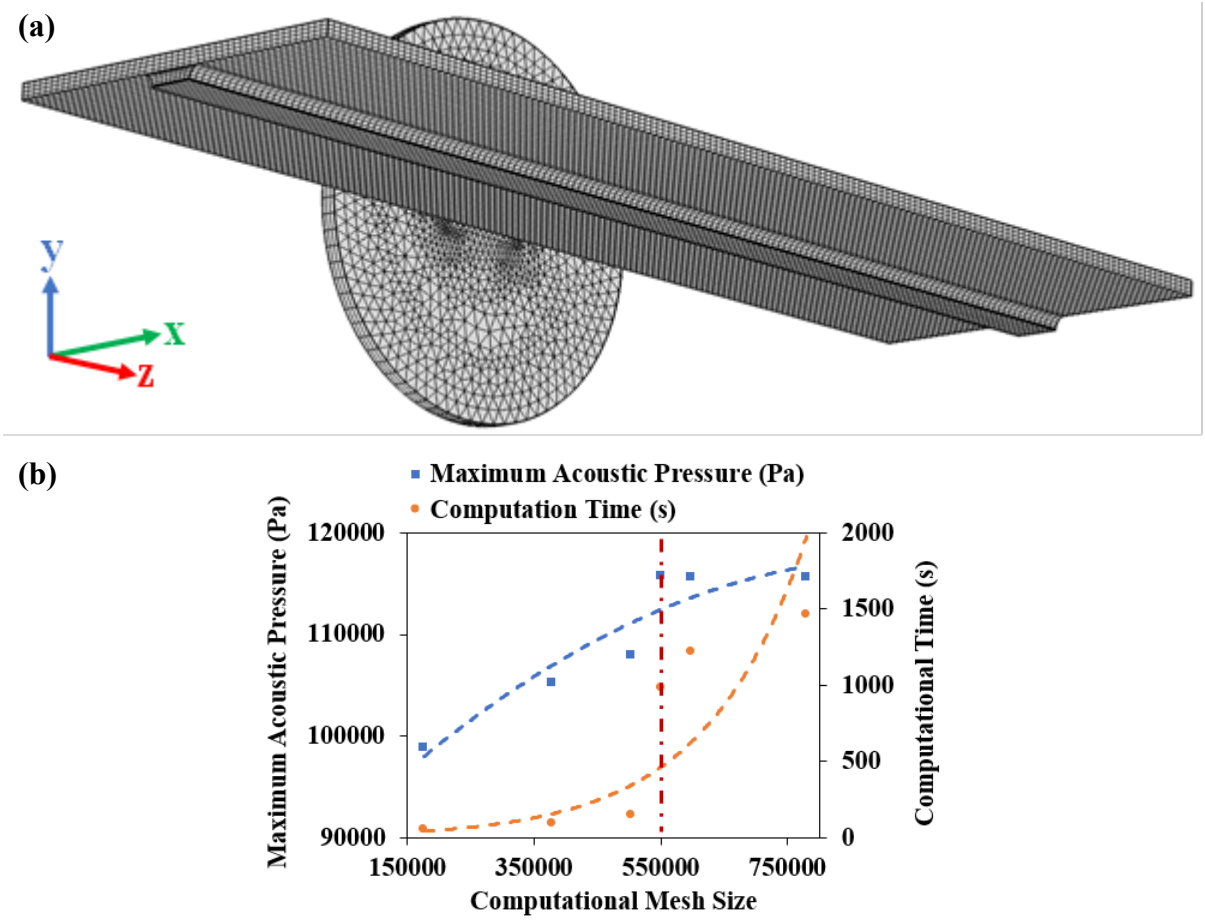

Figure 2 (a) Modelled geometry and computational mesh for a side mounted PZT setup, **(b)** Mesh dependency analysis.

The numerical simulation was performed using the commercial software package COMSOL Multiphysics (5.6) which uses Finite Element Method (FEM) to discretise the governing equations and Newton's iterative method as a solver [14]. The set-up was simulated for a duration of 5 s and with a time step of 0.001 s as the solution converged with convergence criteria of 10^{-6}. The results obtained from the simulations were then compared to the

experimental data for the purpose of verification and explanation of the results. The exhaustive details on the analytical and numerical investigation of the current continuous-flow capillary bridge acoustofluidics system can be found in [18].

4 Results and Discussions

4.1 Particle Patterning in Continuous-Flow Capillary Bridge Channels

Figure 3 presents the results of **(a)** experimental yeast particle alignment and **(b)** numerical simulations of acoustic pressure field inside a capillary bridge channel with a width of 2.5 mm, a height of 0.75 mm and a continuous flow rate of 2.5 µl/s from top view using two different frequencies of **(1)** 1.035 MHz and **(2)** 3.34 MHz. In the simulated acoustic pressure field, the blue and red colours show the minimum and maximum values of the acoustic pressure, respectively, and the white colour shows the pressure nodes.

The results show that during the experiments, yeast particles aligned into continuous parallel lines (**Figure 3(a)**) that closely follows the pressure node lines of the acoustic pressure field in water (**Figure 3(b)**). This is expected as explained in the previous section. The distance between each two adjacent line is equal to the half of the acoustic wave's wavelength. At the higher frequency (see **Figures 3(a-2)** and **(b-2)**) as the wavelength decreases, the number of lines which the yeast particles formed increases. The lines still follow the pressure node line patterns.

Although there are some gaps in the pressure node lines (visible in **Figure 3(b)**), the yeast alignment spans these gaps to form unbroken lines (as seen **Figure 3(a)**) due to the presence of the fluid flow. In other words, the node lines of the acoustic pressure field may not necessarily form continuous lines, but the particles continuously flow and form the linear patterns due to the existence of the continuous fluid flow. At lower flow rates, the yeast lines can become more distorted and irregular corresponding to the gaps in the pressure node line patterns.

It has been shown [10] that the pressure nodes formed in the wave-guide extend across the solid-fluid interface into the water of the capillary bridge to create the pressure nodes seen in **Figure 3(b).** The distance between adjacent pressure node lines was shown to decrease in water compared to the pressure node patterns.

(a-1)

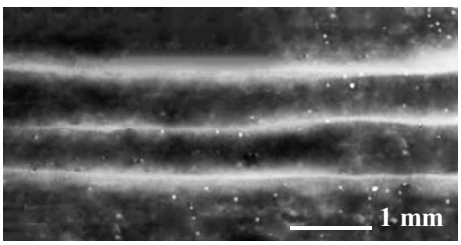

(b-1)

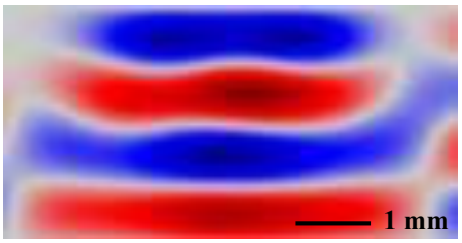

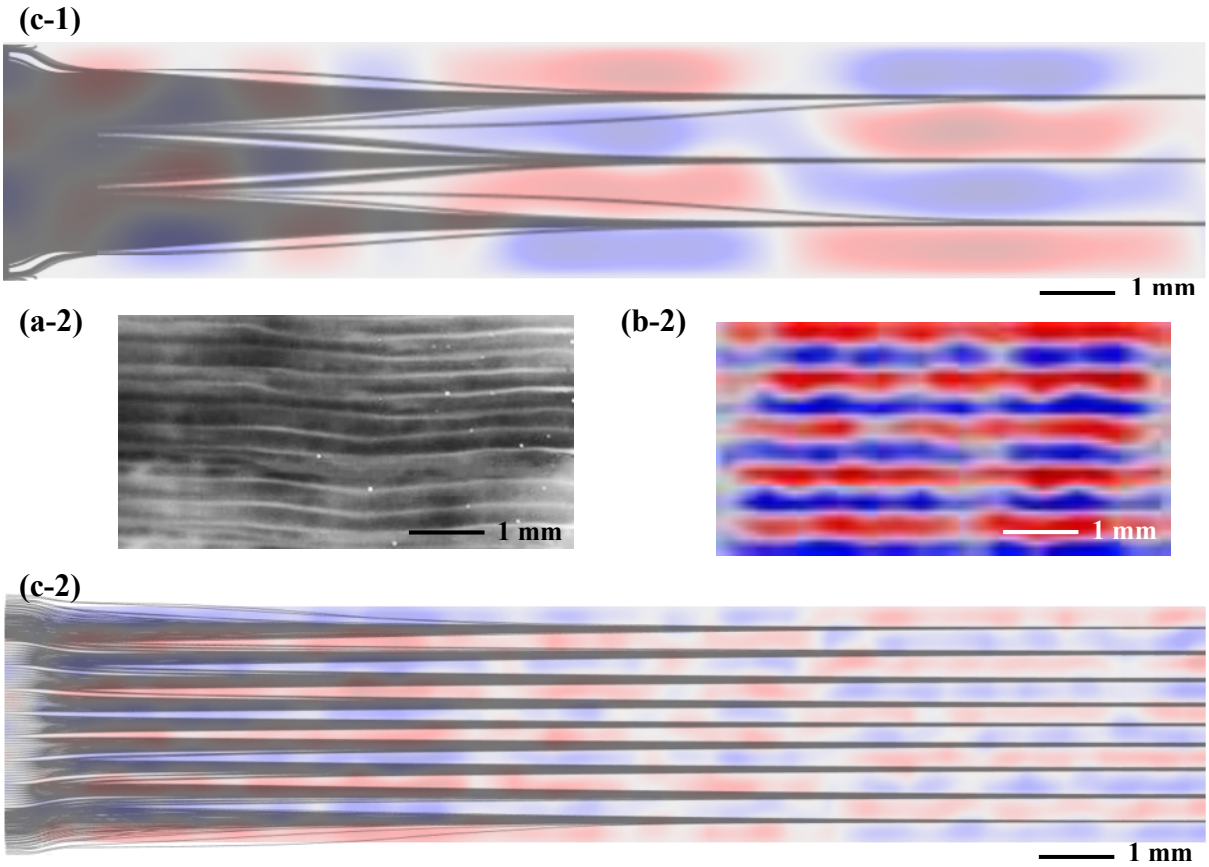

Figure 3 *Top views of* ***(a)*** *experimental yeast particle alignment, numerically simulated* ***(b)*** *acoustic pressure field in water, and* ***(c)*** *particle tracks from top view directly in front of the side-mounted PZT disk in a 2.5 mm wide and 0.75 mm high continuous-flow capillary bridge channel with a 2.5 µl/s flow rate and a frequency of* ***(1)*** *1.035 MHz and* ***(2)*** *3.34 MHz.*

Patterning of the yeast particles inside a continuous-flow capillary bridge channel with a width of 18 mm and a height of 0.75 mm height from the top view is shown in **Figure 4**. Two ultrasound frequencies of 1.035 MHz (**Figure 4(a)**) and 3.34 MHz (**Figure 4(b)**) and a flow rate of 2.5 µl/s were applied to the system.

Compared to particle alignment inside the 2.5 mm wide channel (**Figure 3**), particle lines in the 18 mm wide channel are slightly distorted when the frequency of 1.035 MHz is applied. The line become significantly distorted as the frequency increases to 3.34 MHz. Increasing the fluid flow rate inside the capillary bridge channel smoothens the particle patterns and converts some of the distorted patterns into straight line as the particles flow inside the channel along with the liquid.

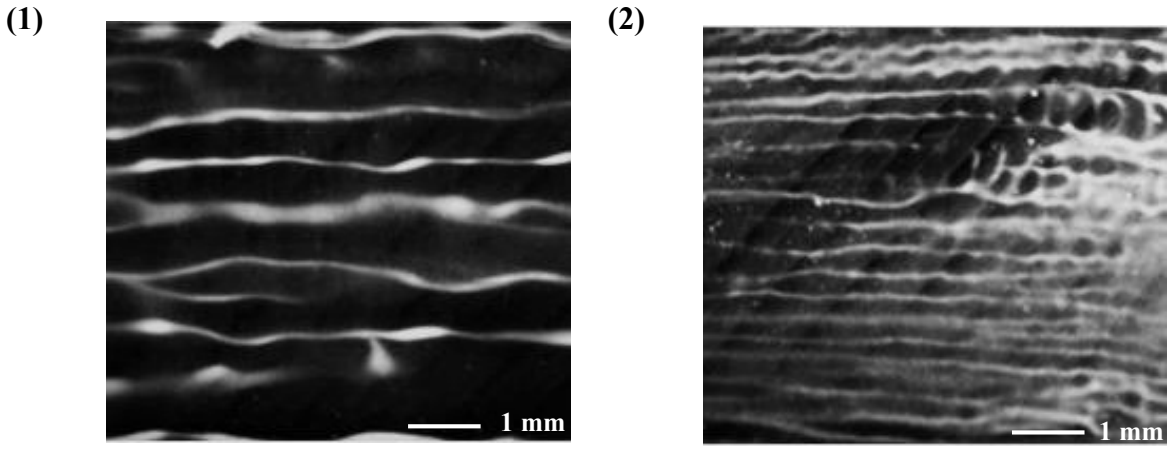

Figure 4 *Top views of experimental yeast particle patterning in water directly in front of the side-mounted PZT disk in an 18 mm wide and 0.75 mm high continuous-flow capillary bridge channel with a 2.5 µl/s flow rate and a frequency of* ***(1)*** *1.035 MHz and* ***(2)*** *3.34 MHz.*

4.2 Effects of Channel Geometry on Particle Patterning

To study the effects of channel geometry on the patterning of yeast particles within the acoustic field inside the capillary bridge, the same acoustofluidic set-up but without a liquid flow was utilised. The no-flow condition was enforced in order to enable the investigation of the key effects of various geometries of the fluid-guide on the acoustofluidic system. **Figure 5** shows the results of **(a)** experimental yeast particle patterning and **(b)** numerical simulations of acoustic pressure field inside two configurations of the capillary bridge channel with **(1)** a width of 3 mm and 10-degree angle relative to the PZT and **(2)** tapered configuration with the narrow end of 4 mm and wide end of 6 mm, both with a 0.75 mm height and a frequency of 1.035 MHz.

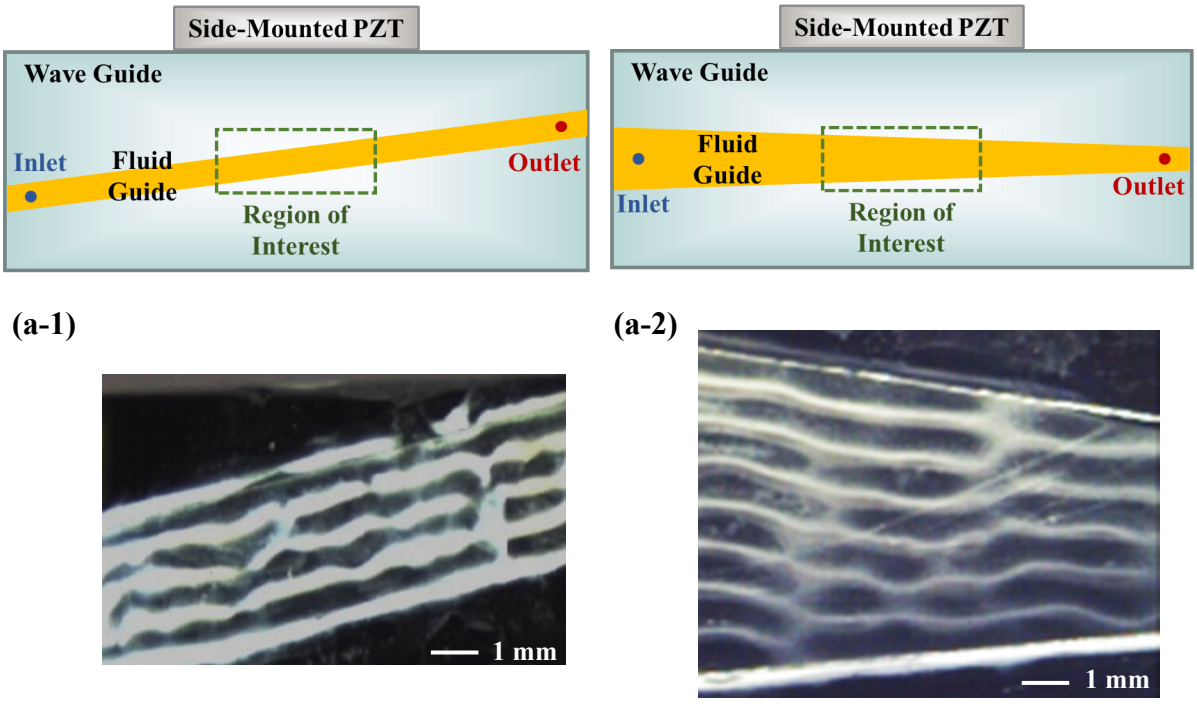

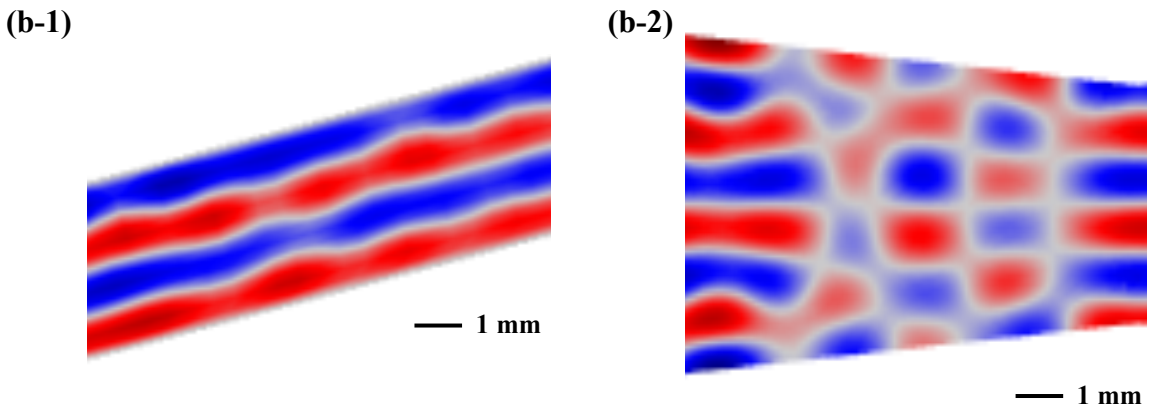

Figure 5 *Top views of* ***(a)*** *experimental yeast particle patterning and* ***(b)*** *numerically simulated acoustic pressure field in water directly in front of the side-mounted PZT disk in a* ***(1)*** *3 mm wide channel with a 10-degree angle relative to the PZT and* ***(2)*** *tapered configuration with the small base of 4 mm and large base of 6 mm, both with a 0.75 mm height and a frequency of 1.035 MHz.*

It has been reported that for capillary tubes [29,30] where there is a wall surrounding the entire channel and capillary bridges [13], the node direction is defined by the edge of the channel and not by the PZT direction. We also observed pressure node lines form parallel to the edge of the channel (the air-water interface) and thus the yeast particles are aligned parallel to the air-water interface of the capillary bridge as shown in **Figures 5(a-1)** and **(b-1)**. This is due to the edge of the water being step change in mass loading of the solid wave-guide [10]. Mass loading reduces the wavelength in solids. The step change does not extend across the whole slide depth but refracts the waves near the water interface. The refracted waves are unlikely to form a resonance but like interacting circular waves, they form standing waves and nodes.

To further investigate whether the nodes are initially formed in the wave-guide or the water, a tapered channel was utilised to create the capillary bridge channel. The angled edges of the tapered channel prevent the creation of a strong resonance in the water. The results produced two alternative cases. Experimental results could switch between the two cases over two apparently identical consecutive runs. In Case 1, the nodes form parallel to the water-air interface as shown in **Figures 5(a-2)**. In Case 2, a checkerboard pattern formed with the acoustic pressure node lines parallel to the direction of the wave-guide instead of the edge of the capillary bridge channel as shown in **Figures 5(b-2)**. Note Case 1 also occurs with simulations and Case 2 also occurs with experiments, these are not shown here. The two different acoustic pressure node patterns observed above, either parallel to the edges of the capillary bridge (**Figures 5(a-1), (b-1)** and **(a-2)**) or the edge of the wave-guide (**Figures 5 (b-2)**), can be reconciled if the nodes are formed by wave interference producing standing waves in the wave-guide as opposed to a resonance somehow forming in the water. This is because in the solid, the non resonant standing waves can arise from a variety of interfaces while in the water the edge of the channel is the only interface. The strongest interference pattern in the solid wave-guide is usually the one aligned to the step in mass loading at edge of the water (**Figures 5(a-1), (b-1)** and **(a-2)**). However, when the channel edges are not parallel to each other, waves from the mass loading step will form weak or no standing waves and instead the waves from the outer boundaries of the wave-guide provide the dominant standing waves in the observed pattern of wave-guide **Figure 5 (b-2)**.

4.3 Effects of Channel Width on Acoustic Pressure Field

The acoustic pressure field for four capillary bridge channels with widths of **(1)** 1 mm, **(2)** 5 mm, **(3)** 10 mm, and **(4)** 15 mm were numerically simulated with a fixed frequency of 1.035 MHz. The obtained top views are presented in **Figure 6**. For the 1 mm wide channel (**Figure 6(1)**), the acoustic pressure nodes are formed perpendicular to (but not along the) capillary bridge channel edges. Since the width is less than one wavelength, the pressure nodes cannot form along the channel, but the waves aligned by the ends orientated with the sides of the wave-guide create the pressure nodes that cross the channel. When a slightly wider fluid-guide (e.g., 2.5 mm or 3 mm wide as shown in previous sections) is selected, the pressure nodes are patterned linearly and parallel to air-water edges of the capillary channel. By increasing the channel width to 5 mm (**Figure 6(2)**), the pressure nodes are formed along the channel by the edges of the capillary bridge. The pressure node lines are more pronounced in the centreline of the channel whereas weaker pressure nodes perpendicular to the length of the channel disturb the linear pattern of parallel pressure nodes at the edges of the channel. Further increase in the channel width to 10 mm (**Figure 6(3)**) results in formation of pressure nodes in various directions resembling a checkerboard pattern. In the widest channel with a width of 15 mm (**Figure 6(4)**), the pressure nodes present a 3×10 grid of linear lines at right angles. However, the 10 nodes across the channel are not equally spaced. They are probably formed by two independent interfaces orientating the waves, i.e., one between the long edges of the wave-guide, and the other between the boundaries of the capillary bridge pinned to the wave-guide.

With the above information, the width of the capillary bridge channel can be optimised for a set frequency to realise particle alignment. Here for the frequency of 1.035 MHz the optimum capillary bridge with can be found to be between 0.5 mm and 2.0 mm.

With the wave-guide (the first glass slide) still in place, replacing the polystyrene fluid-guide with a second microscope slide to act as a new fluid-guide, the maximum width of 25 mm (which is the width of the wave-guide) for the capillary bridge channel can be achieved. **Figure 7** presents the results of **(a)** experimental yeast particle alignment and **(b)** numerical simulations of acoustic pressure field inside the 2 mm wide capillary bridge channel with a height of 0.75 mm from top view using four different frequencies of **(1)** 1.035 MHz and **(2)** 3.34 MHz, **(3)** 5.57 MHz, and **(4)** 7.58 MHz frequency. In these wide channels, the pattern produced by the yeast particles resembles a checkerboard pattern because two interfaces at right angles waves are producing waves of near equal magnitude. The waves get disrupted as they travel from the interface by the minor reflections and losses to the water leading to a checkboard pattern with very rounded corners.

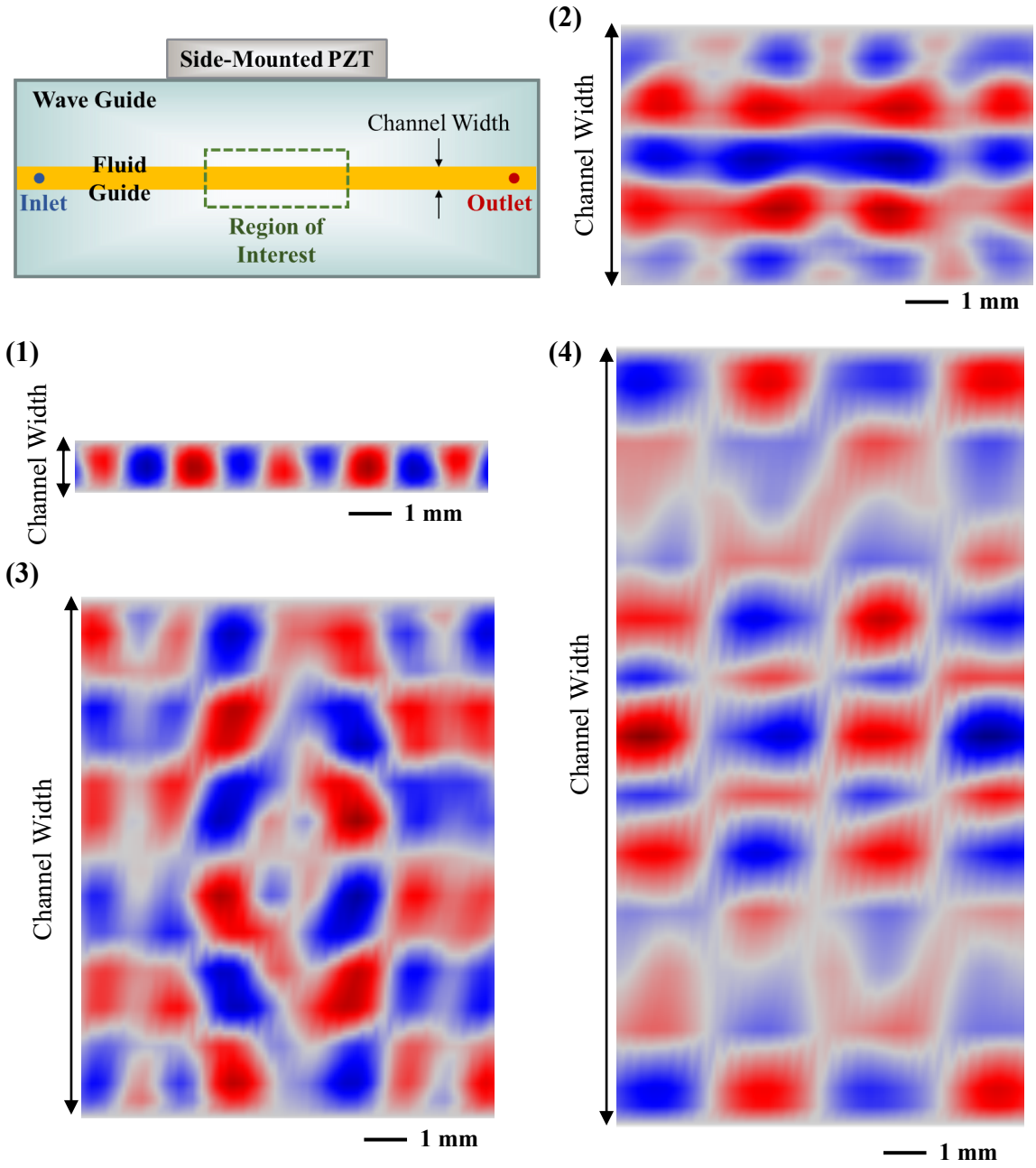

Figure 6 *Top views of numerically simulated acoustic pressure field in water directly in front of the side mounted PZT disk in a* ***(1)*** *1 mm,* ***(2)*** *5 mm,* ***(3)*** *10 mm, and* ***(4)*** *15 mm wide channel all with a 0.75 mm height and a frequency of 1.035 MHz.*

Additionally, as the frequency increases the distance between the pressure node lines decreases as can be seen in **Figure 7**. This is expected since the distance between each two adjacent line is theoretically equal to the half of the acoustic wavelength and both experimental data and numerical simulation results are in good agreement.

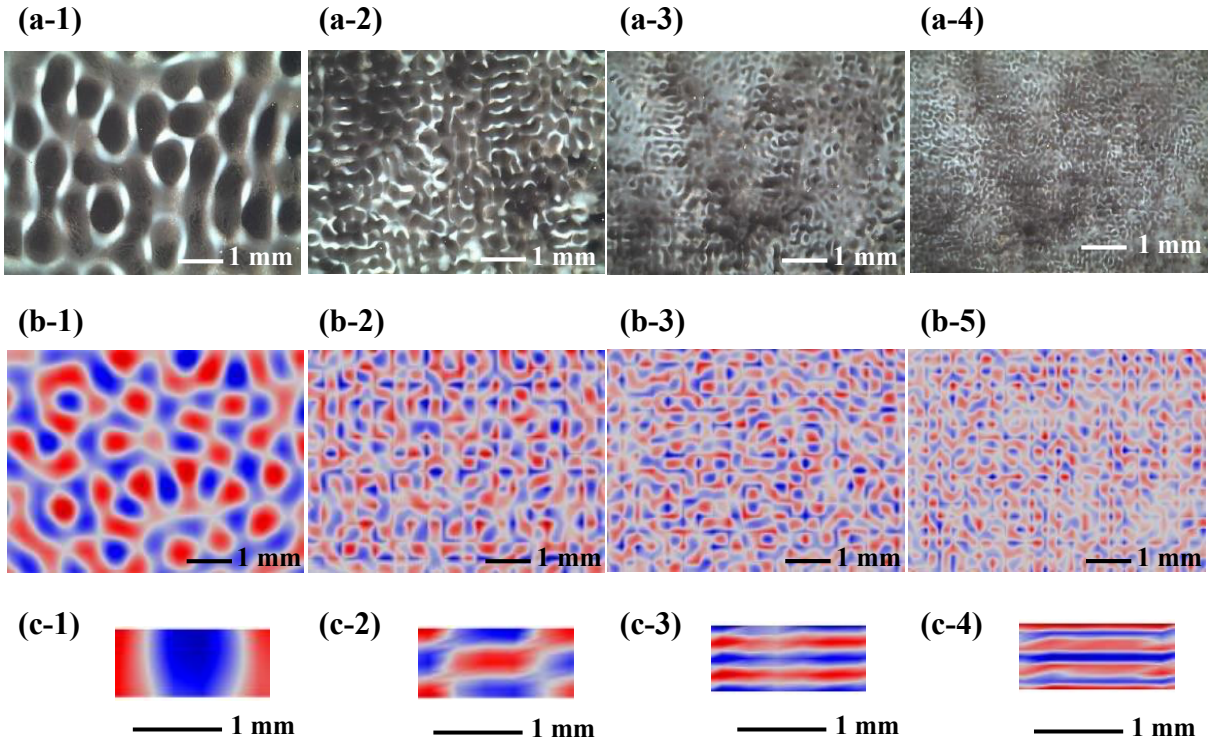

***Figure** 7 Top views of **(a)** experimental yeast particle patterning and **(b)** numerically simulated acoustic pressure field in water and **(c)** side-view of numerically simulated acoustic pressure field in water directly in front of the side mounted PZT disk in a 25 mm wide and 0.75 mm high capillary bridge channel with a frequency of **(1)** 1.035 MHz, **(2)** 3.34 MHz, **(3)** 5.57 MHz, and **(4)** 7.58 MHz.*

Within the height of the capillary bridge channel, the pressure nodes lines are vertical at the frequency of 1 MHz, however, above 1 MHz frequency, the pressure node lines turn parallel to the glass slides. This flip in direction occurs when the water depth is larger than half of the wavelength and was achieved here by increasing the frequency. Therefore, when the wavelength is less than two times the channel height, the waves are reflected from the upper surface to form a fluid resonance in a plane normal to the wave-guide, and the pressure node patterns presented in **Figure 7 (c-3) and (c-4)** are created.

Figure 8 presents the comparison of the average distances of the checker-board patterns of yeast particles at different frequencies driven by the PZT disk. The theoretical results (estimated based on Equation: $D = \frac{\lambda}{2}$), experimental results and simulation results show good agreements among each other. As the frequency increases, the average distance between the yeast particle patterns decreases (which is still corresponding to about half of the wavelength of the acoustic wave in the glass).

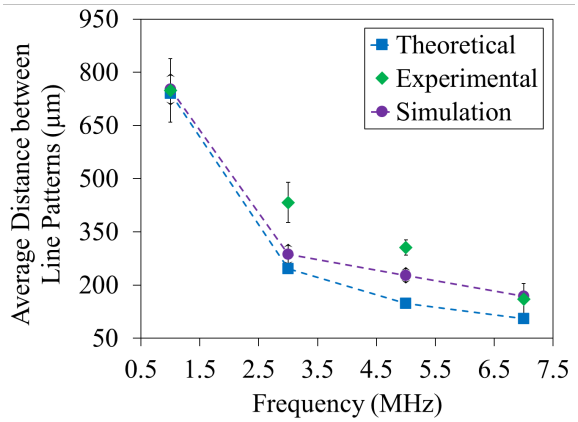

Figure 8 *Comparison of the theoretical, experimental and simulation results for the distances between the yeast particle patterns in water in placed between two glass slides using a side driven PZT disk with different frequencies of 1.035 MHz, 3.34 MHz, 5.57 MHz, and 7.58 MHz.*

5 Conclusions

In this paper, a continuous-flow acoustofluidic system was proposed which utilises a capillary bridge between a wave-guide and a fluid-guide to create a wall-less channel. A PZT disk was used as the acoustic wave source for the acoustic manipulation and patterning of yeast particles. Yeast particles were successfully aligned parallel to the edges of the capillary bridge as they flowed inside the wall-less channel. The continuous flow inside the capillary bridge channel smoothened the linear particle pattens into straight lines parallel to the channel edges. The generated particle patterns at various frequencies, channel geometries and widths were experimentally and numerically investigated. The proposed numerical model produced similar results to the experimental data. It was shown that the particles form linear patterns parallel to the air-water edges of the channel, instead of corresponding to the direction of the surface of the PZT disk. The width of the fluid-guide (or channel) showed to have a significant effect on the acoustic pressure fields and thus the particle patterns. When the channel width was smaller than half of acoustic wavelength in water, no pressure node line was formed inside the channel. Whereas increasing the channel width beyond 2.5 wavelengths in water resulted in the particle pattern lines becoming significantly distorted. Choosing the channel width within a proper range realised particle patterning inside the capillary bridge channel, while the liquid flow smoothed the particle lines. It was concluded that at 1.035 MHz, the optimum width for obtaining the particle alignment was between 0.5 mm and 2.0 mm.

Acknowledgements

This work was supported by the Engineering and Physical Sciences Research Council of UK (EPSRC EP/P018998/1) and partially from the UK Fluids Network Special Interest Group of Acoustofluidics (EP/N032861/1).

References

[1] J. Shi, D. Ahmed, X. Mao, S.-C. S. Lin, A. Lawit, and T. J. Huang, "Acoustic Tweezers: Patterning Cells and Microparticles Using Standing Surface Acoustic Waves (SSAW)," *Lab*

on a chip, vol. 9, no. 20, pp. 2890-2895, 2009.

[2] K. Wang, W. Zhou, Z. Lin, F. Cai, F. Li, J.-r. Wu, L. Meng, L. Niu, and H. Zheng, "Sorting of Tumour Cells in a Microfluidic Device by Multi-Stage Surface Acoustic Waves," *Sensors and Actuators B: Chemical,* vol. 258, pp. 1174-1183, 2017.

[3] T. Franke, S. Braunmuller, L. Schmid, A. Wixforth, and D. A. Weitz, "Surface Acoustic Wave Actuated Cell Sorting (SAWACS)," *Lab on a chip,* vol. 10, no. 6, pp. 789-94, Mar 21 2010.

[4] L. Schmid, D. A. Weitz, and T. Franke, "Sorting Drops and Cells with Acoustics: Acoustic Microfluidic Fluorescence-Activated Cell Sorter," *Lab on a chip,* vol. 14, no. 19, pp. 3710-3718, 2014.

[5] J. Nam, H. Lim, D. Kim, and S. Shin, "Separation of Platelets from Whole Blood Using Standing Surface Acoustic Waves in a Microchannel," (in eng), *Lab on a chip,* vol. 11, no. 19, pp. 3361-4, Oct 7 2011.

[6] M. Wu, K. Chen, S. Yang, Z. Wang, P.-H. Huang, J. Mai, Z.-Y. Li, and T. J. Huang, "High-Throughput Cell Focusing and Separation via Acoustofluidic Tweezers," *Lab on a chip,* vol. 18, no. 19, pp. 3003-3010, 2018.

[7] Y. Ai and B. L. Marrone, "Separation of Biological Cells in a Microfluidic Device Using Surface Acoustic Waves (SAWs)," in *SPIE MOEMS-MEMS*, 2014, vol. 8976: SPIE, p. 7.

[8] F. Petersson, A. Nilsson, C. Holm, H. Jonsson, and T. Laurell, "Separation of Lipids from Blood Utilizing Ultrasonic Standing Waves in Microfluidic Channels," (in eng), *The Analyst,* vol. 129, no. 10, pp. 938-43, Oct 2004.

[9] Guo, F., Li, Z., & Liu, Y. (2023). "Automated separation of platelet-reduced plasma using acoustofluidic systems." Microsystems & Nanoengineering, 9(10), 134–145. DOI:10.1038/s41378-022-00435-6.

[10] J. Nam, H. Lim, C. Kim, J. Yoon Kang, and S. Shin, "Density-Dependent Separation of Encapsulated Cells in a Microfluidic Channel by Using a Standing Surface Acoustic Wave," (in eng), Biomicrofluidics, vol. 6, no. 2, pp. 24120-2412010, Jun 2012, doi: 10.1063/1.4718719.

[11] R. Tao et al., "Thin Film Flexible/Bendable Acoustic Wave Devices: Evolution, Hybridization and Decoupling of Multiple Acoustic Wave Modes," Surface and Coatings Technology, vol. 357, pp. 587-594, 2019.

[12] Li, P., Liu, C., & Zhang, L. (2023). "Advances in acoustofluidic particle and cell manipulation." Biophysical Reviews, 15(2), 89–103. DOI:10.1007/s12551-023-01112-2.

[13] J. J. Hawkes, S. Maramizonouz, C. Jia, M. Rahmati, T. Zheng, M. B. McDonnell, YQ. Fu, Node formation mechanisms in acoustofluidic capillary bridges, Ultrasonics, Volume 121, 2022, 106690.

[14] M. H. Panhwar et al., "High-Throughput Cell and Spheroid Mechanics in Virtual Fluidic Channels," Nat Commun, Research Support, Non-U.S. Gov't vol. 11, no. 1, p. 2190, May 4 2020, doi: 10.1038/s41467-020-15813-9.

[15] W. Lee, Y. Heo, and S. Takeuchi, "Wall-Less Liquid Pathways Formed with Three-Dimensional Microring Arrays," Applied Physics Letters, vol. 101, no. 11, p. 114108, 2012.

[16] R. Renaudot et al., "A Programmable and Reconfigurable Microfluidic Chip," Lab on a chip, vol. 13, no. 23, pp. 4517-4524, 2013.

[17] C. Devendran, T. Albrecht, J. Brenker, T. Alan, and A. Neild, "The Importance of Travelling Wave Components in Standing Surface Acoustic Wave (SSAW) Systems," *Lab on a chip,* vol. 16, no. 19, pp. 3756-3766, 2016.

[18] S. Maramizonouz, (2021) Numerical and experimental study of interactions between surface acoustic waves, fluids, and particles in acoustofluidic systems. Doctoral thesis, Northumbria University.

[19] W. L. Nyborg, "Acoustic Streaming due to Attenuated Plane Waves," The Journal of the Acoustical Society of America, vol. 25, no. 1, pp. 68-75, 1953, doi: 10.1121/1.1907010.

[20] J. Lighthill, "Acoustic Streaming," Journal of Sound and Vibration, vol. 61, no. 3, pp. 391-418, 1978, doi: 10.1007/s001620050068.

[21] H. Bruus, Theoretical Microfluidics. Oxford university press Oxford, 2008.

[22] G. K. Batchelor, An Introduction to Fluid Dynamics (Cambridge Mathematical Library). Cambridge: Cambridge University Press, 2000.

[23] COMSOL, "COMSOL User's Guide," 5.6 ed, 2018.

[24] C. T. Crowe, J. D. Schwarzkopf, M. Sommerfeld, and Y. Tsuji, Multiphase Flows with Droplets and Particles. CRC press, 2011.

[25] L. V. King, "On the Acoustic Radiation Pressure on Spheres," Proceedings of the Royal Society of London. Series A-Mathematical and Physical Sciences, vol. 147, no. 861, pp. 212-240, 1934.

[26] K. Yosioka and Y. Kawasima, "Acoustic Radiation Pressure on a Compressible Sphere," Acta Acustica united with Acustica, vol. 5, no. 3, pp. 167-173, 1955.

[27] A. Doinikov, "Acoustic Radiation Pressure on a Rigid Sphere in a Viscous Fluid," Proceedings of the Royal Society of London. Series A-Mathematical and Physical Sciences, vol. 447, no. 1931, pp. 447-466, 1994.

[28] A. Doinikov, "Acoustic Radiation Pressure on a Compressible Sphere in a Viscous Fluid," Journal of Fluid Mechanics, vol. 267, pp. 1-22, 1994.

[29] S. Maramizonouz, C. Jia, M. Rahmati, T. Zheng, Q. Liu, H. Torun, Q. Wu, and Y. Fu, "Acoustofluidic Patterning inside Capillary Tubes Using Standing Surface Acoustic Waves," *International Journal of Mechanical Sciences,* vol. 214, p. 106893, 2022.

[30] Q. Wang, S. Maramizonouz, M. Stringer Martin, J. Zhang, HL Ong, Q. Liu, X. Yang, M. Rahmati, H. Torun, WP. Ng, Q. Wu, R. Binns, YQ Fu, Acoustofluidic patterning in glass capillaries using travelling acoustic waves based on thin film flexible platform, Ultrasonics, Volume 136, 2024, 107149.